Biochimica et Biophysica Acta 1798 (2010) 318–326

Contents lists available at ScienceDirect

Biochimica et Biophysica Acta

journal homepage: www.elsevier.com/locate/bbamem

Dynamic and energetic mechanisms for the distinct permeation rate in AQP1 and AQP0

Hu Qiu, Shaojie Ma, Rong Shen, Wanlin Guo *

Institute of Nano Science, Nanjing University of Aeronautics and Astronautics, Nanjing 210016, China

ARTICLE INFO

Article history:
Received 4 May 2009
Received in revised form 27 October 2009
Accepted 14 November 2009
Available online 2 December 2009

Keywords:
Aquaporin
Molecular dynamics
Water conduction
Energetic mechanism

ABSTRACT

Despite sharing overall sequence and structural similarities, water channel aquaporin 0 (AQP0) transports water more slowly than other aquaporins. Using molecular dynamics simulations of AQP0 and AQP1, we find that there is a sudden decrease in the distribution profile of water density along the pore of AQP0 in the region of residue Tyr23, which significantly disrupts the single file water chain by forming hydrogen bond with permeating water molecules. Comparisons of free-energy and interaction-energy profiles for water conduction between AQP0 and AQP1 indicate that this interruption of the water chain causes a huge energy barrier opposing water translocation through AQP0. We further show that a mutation of Tyr23 to phenylalanine leads to a 2- to 4-fold enhancement in water permeability of AQP0, from $(0.5\pm 0.2)\times 10^{-14}$ cm^3s^{-1} to $(1.9\pm 0.6)\times 10^{-14}$ cm^3s^{-1}. Therefore, Tyr23 is a dominate factor leading to the low water permeability in AQP0.

1. Introduction

Water transport across biological membranes is essential to cellular functions. Since lipid bilayers exhibit limited water permeability, a family of membrane channels, named aquaporins (AQPs), provides an efficient pathway facilitating water permeation [1,2]. Driven by osmotic gradient, water molecules can pass passively through these transmembrane channels, which have been found and characterized in a broad range of life-forms. In terms of their selectivity, these proteins can be mainly divided into two subfamilies: conduct water only (aquaporins); transport water plus some small neutral solutes such as glycerol and urea (aquaglyceroporins) [1-3].

Recently, a number of atomic structures of AQPs from different cells have been determined [4-9]. They display a high conservation of general architecture structure, and form homotetramers in cell membranes with each monomer consisting of six transmembrane helices and two half-membrane-spanning loops. The four transmembrane channel pores formed independently by each monomer can be divided into three parts: an extracellular vestibule, a long narrow pore (selectivity filter) containing the constriction region, and a cytoplasmic vestibule. On the basis of these atomic structures, real-time all atoms molecular dynamics (MD) simulations have been widely employed to investigate water dynamics in AQPs, and have provided new insights into the mechanism of permeation and selectivity of AQPs [10–15].

Despite the high similarity in overall architecture among AQPs, they display a wide range of permeabilities, selectivities, and other dynamic characteristics [1,2]. For instance, as the major integral membrane protein of the lens fiber cells, AQP0, which plays a critical role in maintaining a healthy lens, transports water more slowly than other AQPs such as AQP1 [16], which was characterized as membrane proteins in red blood cells and renal proximal tubules [17]. To maintain lens transparency, it is required that the amount of water in lens fiber cells can be carefully regulated as excess water will destroy the regular structure of crystalline proteins inside the cells. Transparency also requires a sufficiently smaller intercellular space (compare to the wavelength of ambient light) [6,18]. The low permeability of AQP0 is critical to the achievement of these goals. First, AQP0 provides the primary pathway for water movement across lens fiber cell membranes. The low water permeability of AQP0 was suggested to ensure a uniform response to osmotic change by gating of large numbers of the channel proteins such that the content of water in cells can be carefully controlled [6]. Second, AQP0 serves as cell-to-cell adhesion molecules by forming membrane junctions between adjacent cells [1,7,8]. The slow conduction rate of AQP0 may contribute to the stabilization of the membrane junctions by decreasing the risk of junction breakage when water passes through, thus maintaining the intercellular space [18]. Moreover, certain mutations of AQP0 were found to cause congenital cataracts, further showing its critical physiological role in lens fiber cells [19].

Since the high-resolution structures of AQP0 were solved by electron and X-ray crystallography [6-8], studies on determining the structural basis of its slow water conduction have gained much

* Corresponding author. Tel.: +86 25 84891896; fax: +86 25 84895827.
E-mail address: wlguo@nuaa.edu.cn (W. Guo).

0005-2736/$ – see front matter © 2009 Elsevier B.V. All rights reserved.
doi:10.1016/j.bbamem.2009.11.015

attention [10,11,18,20]. Examination of the crystal structures indicates that the significantly narrower pore of AQP0 makes it impossible that AQP0 has a water permeability comparable to AQP1. In particular, two tyrosine residues, Tyr23 and Tyr149, whose side chains protrude directly into the channel, constrict the AQP0 pore significantly, implying their role in limiting water conduction. MD studies based on these atomic structures suggested that there exists local minima in the average water occupancy profile around the regions of Tyr23 and Tyr149 [10,20], indicating that water passage across these regions are restrained. Furthermore, a recent MD study showed that the lumen-protruding side chains of these two residues impose apparent barriers against water passage, resulting in the slow permeation of AQP0 [18]. However, systematical and detailed understanding of the interactions between the tyrosine residues and permeating water is still lacking. Moreover, which of these key residues plays a dominant role in slowing water flow and how it affects water dynamics and energetics in AQP0 remain unanswered.

In this study, we carried out MD simulations of AQP0 and AQP1 embedded in solvated lipid bilayers, and performed comparative analyses of the water dynamics and energetics for water conduction between AQP0 and AQP1. It is shown that Tyr23, compared to Tyr149, plays a more dominant role in limiting water transport through AQP0 by disrupting the water chain inside the channel pore. To further address this issue, we performed an MD simulation of AQP0 with Tyr23 being replaced by phenylalanine, which is the corresponding residue (Phe24) in AQP1, and found that water permeability was significantly enhanced by the mutation. Furthermore, our simulations also suggest that water dynamics inside AQP0 pore are significantly affected by Tyr23.

2. Materials and methods

2.1. Molecular dynamics simulations

The initial coordinates of AQP1 and AQP0 monomers were taken from published structures in protein data bank (PDB codes: 1YMG for AQP1 [5] and 1J4N for AQP0 [6]), respectively. Tetramers of the proteins were produced using transformation matrices provided in the PDB files. Water molecules inside the channels were kept to maintain the structural stability in initial simulations. Using the program VMD [21], the AQP1 and AQP0 tetramers were embedded in palmitoyl-oleoylphosphatidyl-ethanolamine (POPE) lipid bilayers and solvated by adding water molecules on both sides of the membranes (Fig. 1). The membrane normal was set as the z direction. The starting dimension of the simulation system for AQP1 was 82 Å×82 Å×70 Å composed of 49,084 atoms, and for AQP0 was 89 Å×89 Å×67 Å composed of 55,453 atoms.

All MD simulations were performed by the program NAMD2 [22] using the CHARMM27 force field [23] for the proteins and lipids, and the TIP3P model [24] for water. Periodic boundary conditions were applied in all directions. The particle mesh Ewald (PME) method [25] was employed to treat the long-range electrostatic interactions. Langevin dynamics and the Nose-Hoover Langevin piston method [26] were chosen to maintain the temperature at 310 K and the pressure at 1 atm, respectively. Beginning with 1000 steps energy minimization, both of the systems were simulated for 200 ps, with all C_α atoms of the proteins being constrained with a force constant of 1 kcal/mol/Å^2. Then the proteins were released and further equilibrated for 66 ns. The last 60 ns trajectories were used for analysis. In our simulations, a time step of 2 fs was used and data were recorded every 1 ps.

To further investigate the effect of Tyr23 on limiting water permeation through AQP0, we substituted Tyr23 of AQP0 by phenylalanine, and the mutant system was also simulated for 66 ns as for the wild-type AQP0.

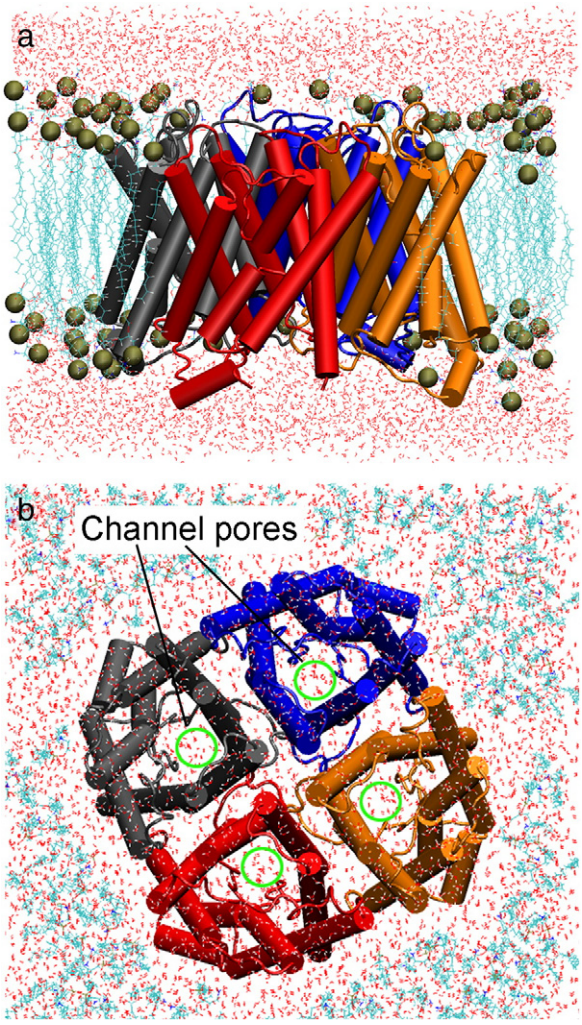

Fig. 1. The simulation system. (a) Side view of the system. Aquaporin tetramer (red, blue, black and orange) is presented in cartoon representation and embedded within a POPE lipid bilayer (cyan) surrounded by water (red dots). Phosphorus atoms are rendered in vdW spheres. For charity some lipid molecules are not shown. (b) Top view of the simulation system.

2.2. Methods for analysis

Analyses were done based on trajectories from the last 60 ns MD simulations. All numeric values to be discussed below were obtained by averaging over the four monomers of the AQP tetramers. For comparison, the center of the conserved NPA motifs in AQPs was set to be $z=0$. The coordinate of oxygen atom of a water molecule was adopted to define the position of water. Along the pore axis z, the channel pore was divided into 0.5 Å thick slabs, and we assume that water molecules in a slab have the same z coordinate. The calculated results here for a position z along the pore axis were obtained by averaging over these water molecules.

2.2.1. Free-energy calculation

For each position z along the pore axis, the relative free-energy profile $G_{PMF}(z)$ (PMF, potential of mean force) is given by [12]

$$G_{PMF}(z) = -k_B T \ln[n(z)] - C \quad (1)$$

Where k_B denotes the Boltzmann constant, $T=310$ K, $n(z)$ is the average number of water molecules whose oxygen atoms are at the position z. The constant C is set to ensure that the global minimum of G_{PMF} equals zero.

2.2.2. Water osmotic permeability

A collective diffusion model was proposed by Zhu et al. [27] to quantify the osmotic permeability P_f of a water channel from equilibrium MD simulations, e.g., carbon nanotubes [27] and AQPs [10,18,28]. In this model, water permeation in a channel is described by a collective coordinate n, which is defined in its differential form, as $dn = \sum_{i \in S(t)} dz_i / L$, where dz_i is the displacement of water molecule i along the pore axis z during a time interval of dt, $S(t)$ denotes the set of water molecules in the channel pore at time t and L is the length of the pore. It is shown that when t is much longer than the velocity correlation time of n, the diffusion constant of n, D_n, can be calculated from the mean square displacement (MSD) of n, $\langle n^2(t) \rangle$, as

$$\langle n^2(t) \rangle = 2D_n t \tag{2}$$

Then one obtains the osmotic permeability P_f of the channel from the relation $P_f = v_w D_n$, where v_w is the average volume of a single water molecule. In our calculations, the trajectory of n for each monomer was divided into 600 short windows, demanding $n(t = t') = 0$ at the stating time t' of each window. $\langle n^2(t) \rangle$ was taken as the average over these windows, as

$$\langle n^2(t) \rangle = \left[\sum_k n_k^2(t) \right] / 600 \tag{3}$$

2.2.3. Single file disruption

As defined by others [14], the disruption of water single file can be quantified by a disruption ratio,

$$dr(z) = W_{\text{disruption}}(z) / W_{\text{total}}(z) \tag{4}$$

where $W_{\text{disruption}}(z)$ and $W_{\text{total}}(z)$ are the total number of disrupted water pairs and the total number of water pairs at position z within the selectivity filter, respectively. If the spacing of a neighboring water pair was longer 199 than 3.75 Å, the water pair was considered disrupted.

2.2.4. Water–Water correlation

Correlated motion of water molecules inside a narrow channel was described by a correlation coefficient $c(z)$, as [12]

$$c(z) = \frac{\langle \Delta z_i \Delta z_j \rangle}{\left(\langle \Delta z_i \Delta z_i \rangle \langle \Delta z_j \Delta z_j \rangle \right)^{1/2}} \tag{5}$$

where $z = 0.5[z_i + z_j]$ denotes the midpoint of oxygen atoms of two neighboring water molecules. Δz_i is defined by $\Delta z_i = z_i(t) - z_i(t + \Delta t)$, and we set $\Delta t = 10$ ps.

2.2.5. Water orientation

For a position z along the pore axis, the bipolar water orientation can be characterized by

$$P(z) = \langle \cos(\theta)_z \rangle \tag{6}$$

where θ is the angle between a water dipole within the channel pore and the pore axis z.

3. Results and discussion

3.1. Comparison of the channel architectures

The atomic structures of AQP1 (PDB: 1J4N) and AQP0 (PDB: 1YMG) have a high degree of similarity. The aqueous pore is mainly lined with hydrophobic residues which are also essential to limit the size of the channel pore. Within the channel pores, two regions play important roles in controlling water conduction and selectivity of the AQPs (Fig. 2). Close to the extracellular vestibule, the aromatic/arginine (ar/R; z~8 Å) site forms the narrowest part of the pores of AQP1 [5], GlpF [9], and AQPZ [29], and was suggested to be essential to channel selectivity [30]. For AQP1(AQP0), the ar/R site is formed by residues Arg197(187), Gly192(182), Phe58(48) and His182(172). The other important region, around the location of the two conserved Asn-Pro-Ala (NPA) motifs, which was considered to be responsible for the inhibition of proton conduction through AQPs [31], lies at the central region of the channel pore. Water dipoles present opposite orientations at the two side of the NPA region, preventing the formation of a "proton wire" in the channel pore and therefore precluding proton conduction through AQPs [31].

Comparison of radius profiles between AQP1 and AQP0 plotted in Fig. 2b shows that AQP0 is remarkably narrower than AQP1 in most regions of the selectivity filter along the pore axis in both the crystal structure and MD simulation. Unlike AQP1, which shows a single constriction (ar/R), two apparent constriction regions in AQP0 pore

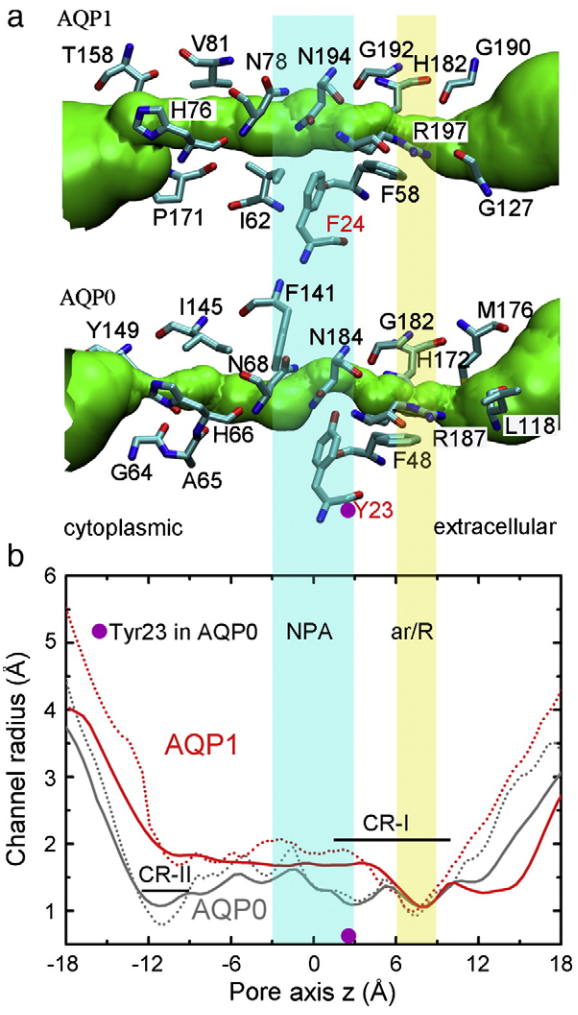

Fig. 2. Channel pores of AQP1 and AQP0. (a) Pore profiles of AQPs. The major residues that form the pores are shown in licorice representation. (b) Comparison of pore radius profiles between AQP1 (red) and AQP0 (gray). The average radius of the channel pore during the last 60 ns simulation is shown in solid curve, whereas dotted curve represents radius yielded from the crystal structure of AQPs (AQP1:1J4N, AQP0:1YMG). The pore axis z is normal to the membrane plane and the center of the NPA motifs is set as the zero point. The purple circle corresponds to the site of Tyr23, and the NPA and ar/R regions are highlighted by cyan and yellow, respectively. Two constriction regions (CR-I, CR-II) in AQP0 are also marked and shown. The pore profiles and radii were prepared with the program HOLE [41], and the coordinate data used for radius calculation were collected every 5 ps.

could be observed: constriction region I around the ar/R site and constriction region II formed by residues Tyr149, Gly64 and Ala65. In the constriction region II, the side chain of Tyr149 extends into the channel pore and narrows the pore radius to ~1 Å. In addition, Tyr23 in the NPA region of AQP0, points its side chain directly into the pore and constricts it significantly (Fig. 2, purple circle). The two tyrosine residues (Tyr23 and Tyr149), which are absent in all fast-conducting AQPs [10,18], were suggested to be responsible for the slow water permeation in AQP0 [6-8,10,11,18,20].

One may note that the average radius profile deviates slightly from the radius profile based on the crystal structure, particularly in the two vestibules. Two factors can explain this deviation. First, the time scale (66 ns) of our MD simulation is apparently long, hence, the configuration changes of residues in the vestibules cannot be avoided. Another dominant factor is that in the calculation of radius, the minimum radius of the pore was taken as a rough measurement. Since the pore has a noncircular profile, the cross-sectional area implied by this calculation could be only treated as an approximate prediction. The range of the selectivity filters of channel pores can be estimated from the pore radius profiles, as $-10<z<8$ Å for AQP1 and $-12<z<8$ Å for AQP0, respectively.

3.2. Channel occupancy and free energies

As shown in previous studies [11,12,14], water molecules were also found to form a highly correlated hydrogen-bonded water chain inside the selectivity filters of AQPs in our simulations. They hop simultaneously to shift the whole single file along the pore axis. Figs. 3a and b display the number of water molecules inside the selectivity filters of AQP1 ($-10<z<8$ Å) and AQP0 ($-12<z<8$ Å) during the last 60 ns MD simulations, respectively. The number of water molecules inside the channel pore of AQP1 varies mostly between 6 and 9, with an average of 7.6 ± 0.4. In the case of AQP0, the channel occupancy varies mostly between 4 and 7, with an average of 5.6 ± 0.5. The large deviation from the average channel occupancy suggests that some pores of the AQP tetramers are instantaneously empty. This observation is in line with previous MD simulations of the glycerol uptake facilitator GlpF, in which some of the four pores formed by the monomers were almost empty at certain time points or periods, whereas the others were filled [14]. The frequent emptying and filling of water were suggested to be attributed to the hydrophobic interiors of the AQP channel pores. Furthermore, in a purely hydrophobic carbon nanotube channel, a similar phenomenon occurs more frequently, demonstrating the role of hydrophobicity of pore wall in controlling the dynamic behaviors of confined water [32].

To gain more details of water binding sites, we show in Fig. 3c the distribution of water density along the pore axis. In general, it is found that the density profiles have many local maxima, each corresponding to a water binding site in the pore, i.e., ~7 sites for AQP1 and ~5 sites for AQP0, respectively, which agrees with the earlier analysis of the channel occupancy. Compared with AQP1, one of missed water binding sites for AQP0 lies at the position $z\sim2.5$ Å, where the mean

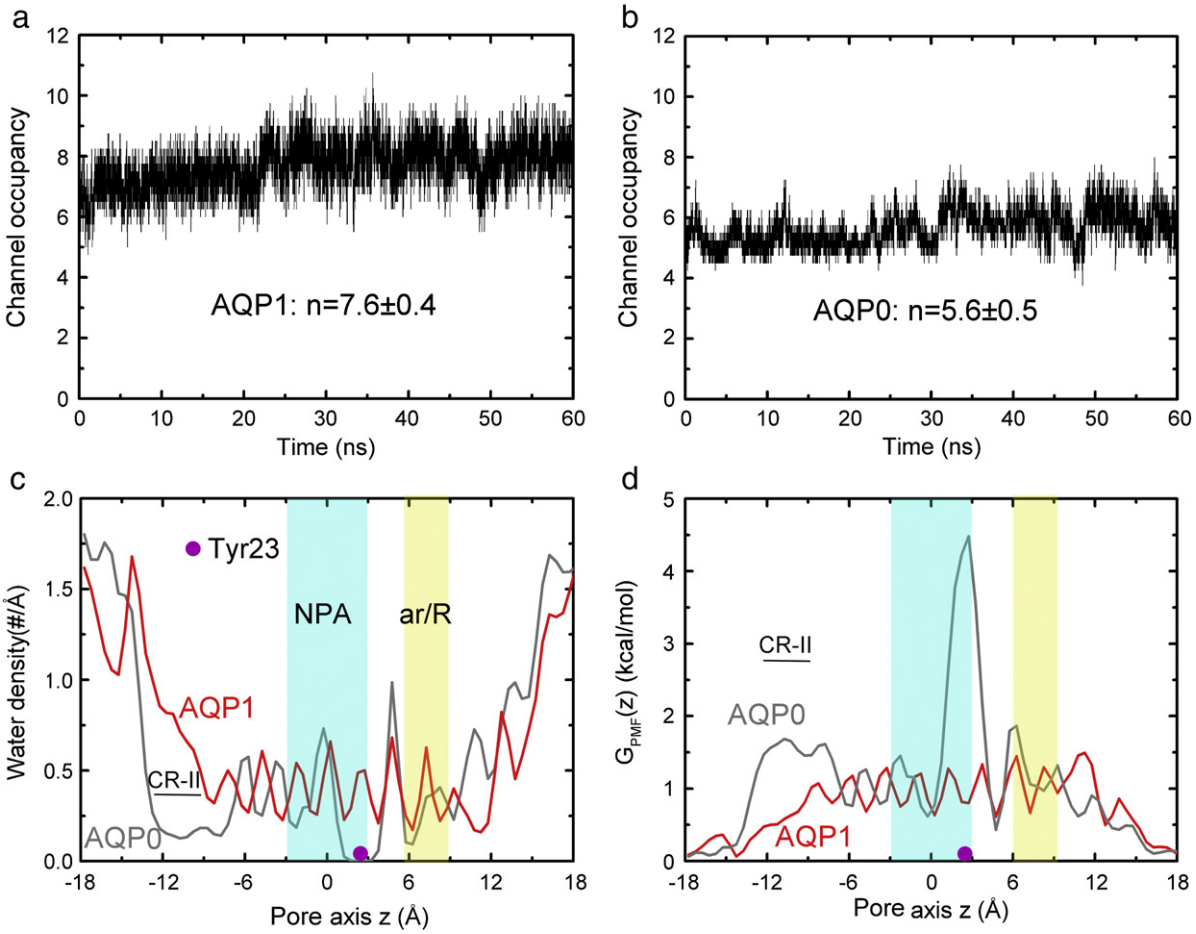

Fig. 3. Water occupancy in AQPs and relative free energies of water permeation through the AQP channels. (a and b) The number of water molecules inside the selectivity filters in the last 60 ns simulation for AQP1 and AQP0, respectively. Means and standard errors were calculated among monomers in each simulation. (c) Distribution of average water density inside the channel pores. The AQP pores were divided into 0.5 Å thick slabs along the pore axis, with the center of each slab corresponding to a position z. The water density here was calculated by measuring the average number of water molecules within the slab at this position during the last 60 ns trajectories of each simulation. (d) Relative free-energy profiles of AQPs.

density decreases to 0.002 $Å^{-1}$, that is, water molecules were observed at this position in only 60 frames of the 60,000 frames MD trajectory (60 ns). Although the pore radius at this position is comparable to the two constrictions (see Fig. 2b), the channel occupancy here is significantly lower than these two constrictions. A very similar arrangement of water molecules in the channel was reported in previous studies [10,20]. Note that the residue Tyr23, is located at this site ($z \sim 2.5$ Å). This tyrosine plugs the channel pore by its OH group hydrogen bonding with permeating waters and reduces water passage through AQP0 [10,18]. In contrast, at the site of Tyr149 ($z \sim -12$ Å), which is part of the constriction region II, the valley in the density profile was relatively shallower than that in the Tyr23 region (see Fig. 3c). Thus, less restriction is imposed on water passage across Tyr149 than across Tyr23.

According to Eq. (1), the relative free-energy $G_{PMF}(z)$ profiles of water permeation through AQP1 and AQP0 were calculated and plotted in Fig. 3d. The selectivity filters of AQP1 and AQP0 contain a series of energy barriers, and there seems no significant difference between AQP0 and AQP1 in most regions of the free-energy curves. For AQP1, since the free-energy profile is rather smooth with slight waving (Fig. 3d, red curve), water molecules encounter sequential barriers against permeation. Water passage through AQP1 is mainly regulated by the combination of these free-energy barriers. However, in contrast to AQP1, two regions with substantially higher barriers against water permeation are noticed in the AQP0 profile. The highest one lies at the site of Tyr23 in AQP0, where water permeation meets a barrier of about 4.48 kcal/mol. Noting that the barrier at the corresponding site in AQP1 is only 0.80–1.00 kcal/mol, there would be a significantly higher energy cost to move a water molecule across the Tyr23 region in AQP0. Different from the largest barrier at Tyr23, in which an abrupt peak of energy barrier is located, the constriction region II, which contains residue Tyr149, displays a few barriers around 1.50 kcal/mol. Recent simulations found that these two tyrosines plug the channel and preclude water flow [10,11,18,20]. Our results here further show that the barrier at Tyr23 site is ~3.0 kcal/mol higher than that around Tyr149, and therefore is a more dominant factor responsible for the low permeability of AQP0.

It should be noted that in the energy analysis parts of this work, i.e., free energy and interaction energy (to be discussed in following sections), a single molecule picture was used, that is, the collective movement of water through AQPs was not taken into account directly. In fact, water movement within the channel occurs in a highly correlated single file configuration. The water chain hops across every free-energy barrier collectively. For instance, when passing across the highest energy barrier around the Tyr23 residue of AQP0, not the water molecule at the barrier itself, but a water chain containing this water molecule hops simultaneously across the barrier.

3.3. Water osmotic permeability

The concerted water movement in AQPs can be described by a collective diffusion model. Here the length of the selectivity filter was taken as the pore length L (18 Å for AQP1 and 20 Å for AQP0, respectively). By averaging over 600 100-ps-wide windows of each trajectory of n, we obtained $\langle n^2(t) \rangle$ from Eq. (3). Then, we calculated the osmotic permeability P_f of each channel pore via D_n obtained from Eq. (2).

Table 1 summarizes reported and our calculated values of single channel water permeability P_f of AQP1 and AQP1. We obtain for AQP1 $P_f = 5.6 \pm 0.5$ (all permeabilities in this paper are in unit of 10^{-14} $cm^3 s^{-1}$). Reported experimental values of P_f for AQP1 vary between 4.6 and 11.7, while simulation results of P_f are 7.1–10.3. Consequently, our result for AQP1 is in good agreement with those in previous studies. For AQP0, we obtain $P_f = 0.5 \pm 0.2$, while reported experimental value is ~0.25. It should be noted, however, the uncertainties in estimating the number of channel proteins per sample may cause large errors in experimental P_f values, which were also concerned by others in previous studies [10,33,34]. This fact implies the little distinction between the present simulation result and the previous experimental values for AQP0 is allowable. Reported P_f of AQP0 based on MD simulations are 0.2 ± 0.2 [10] and 0.28 ± 0.04 [18]. Our computational value based on 60 ns MD simulation is one-fold larger than the reported values, however, taking into account the variety and large errors of calculated results, the amount of the discrepancy is acceptable.

Table 1
Water osmotic permeability.

	P_f ($\times 10^{-14}$ $cm^3 s^{-1}$)	References
AQP1		
Experimental value	4.6~11.7	[36-39]
Simulation result	7.1~10.3	[10,20,33,40]
Present	5.6 ± 0.5	-
AQP0		
Experimental value	0.25	[39]
Simulation result	0.2~0.28	[10,18]
Present	0.5 ± 0.2	–
AQP0-Y23F[a]	1.9 ± 0.6	–

[a] Water permeability for AQP0-Y23F is calculated from MD simulation of the Y23F mutant of AQP0. Means and standard deviations were computed among the monomers in each system.

3.4. Water dynamics inside the channel

As demonstrated in previous studies, water molecules exhibit distinct dynamic behaviors inside the pores of AQP1 and AQP0 [10,20]. Our results in the above sections suggest that Tyr23 plays a key role in limiting water passage through AQP0. Its effect on the water dynamics inside the AQP0 pore can be further determined in details in three aspects: disruption of water single file, water–water correlation and water orientation.

For the hydrogen-bonded single file in the channel pore, we determined its continuity by a parameter called disruption probability (see Section 2.2.3). Fig. 4a plots the disruption probability of hydrogen bonds along the water single file predicted from Eq. (4), showing that large discrepancy exists between AQP1 and AQP0. For AQP1, the profile is fluctuating slightly with a maximum of ~0.20, even in the ar/R region where pore radius constricts to ~1 Å, indicating that the single file is well maintained along the pore axis. In contrast to AQP1, there is a notable disruption peak with a value of 0.99 in the AQP0 profile, which is located at the site of Tyr23 (Fig. 4a, purple circle). At this site, the side chain of Tyr23 forms hydrogen bond with adjacent permeating water, interrupting the hydrogen-bonded water file (Fig. 4d). Since waters permeating through AQP channels are found to form a single file and translocate concertedly, the continuity of the single file is critical to water transport. Hence, the nearly complete disruption of the single file in the Tyr23 region dominantly leads to the slow water permeation through the AQP0 channel, as proposed in the previous free-energy calculations.

The correlation coefficient quantifies the concertedness of water translocation along the channel pore. For each position z along the pore axis, on the basis of Eq. (5), we calculated the correlation coefficient $c(z)$ between neighboring water molecules along the water single file inside the AQP1 and AQP0 pores. Fig. 4b shows that the trend of the correlation profile of AQP1 is similar to that of AQP0. For both AQPs, the water correlation is much higher in the selectivity filters than in the two vestibules. In the selectivity filters, water molecules exist in a form of single file and therefore show a high concertedness between neighboring water molecules. Owing to the expansion of radius in the cytoplasmic and extracellular vestibules (compare to selectivity filter), water molecules within these regions

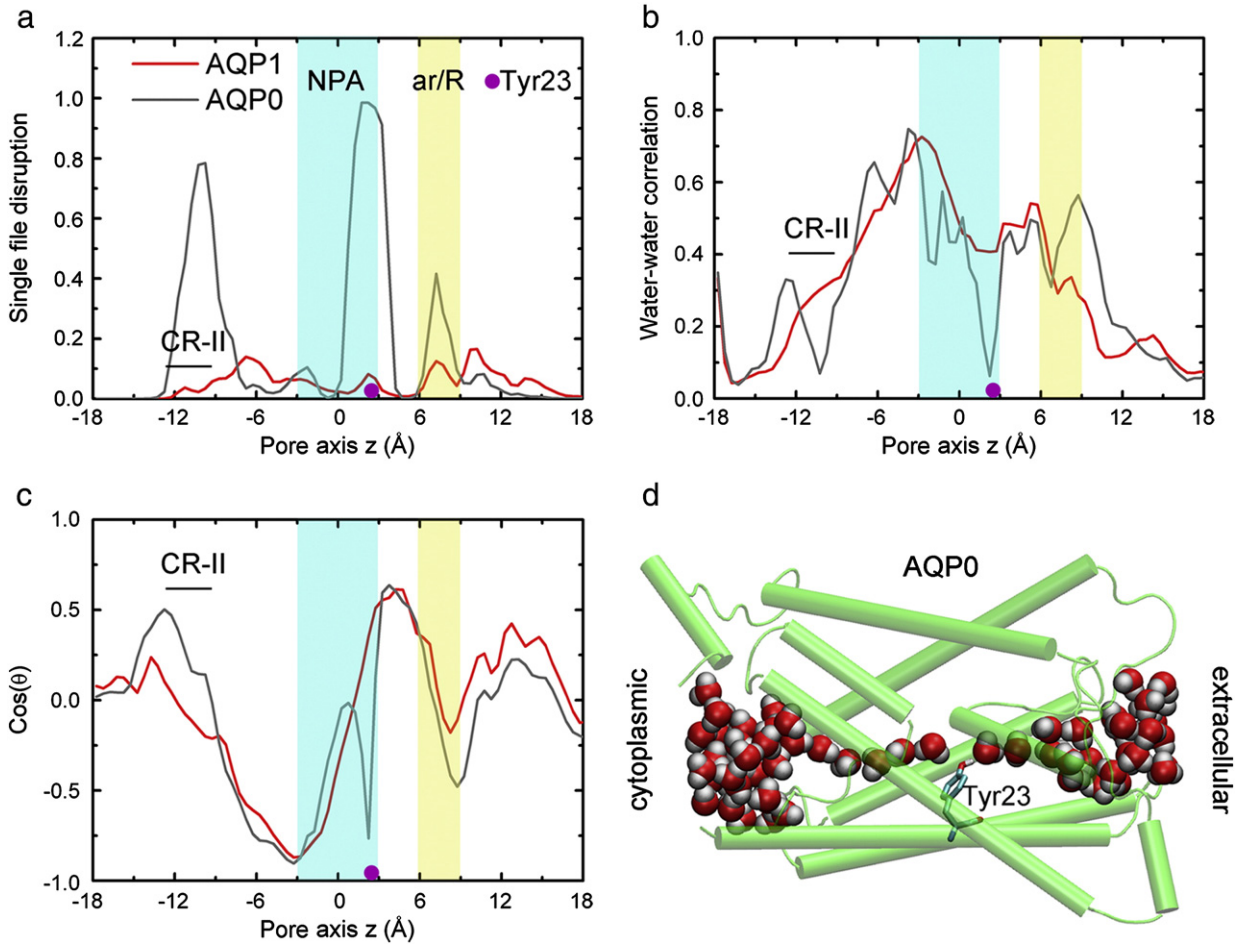

Fig. 4. Characteristic of water inside the AQP pore. (a) The probability distribution of water file disruption inside the channel pore. (b) Water–Water correlation within the pore. (c) Dipole orientation of water molecules within the AQP pore. θ is the angle between a water dipole within the channel pore and the pore axis z. (d) Snapshot from MD simulation presenting the disruption of single file water chain in the AQP0 pore due to Tyr23. Water molecules, the AQP0 protein and its residue Tyr23 are shown in vdW, cartoon and licorice representations, respectively.

present in a bulk-like form rather than the single file configuration, and the hydrogen bonding interactions between water molecules become complicated, thus causing the distinct correlation coefficients in these regions (compare to selectivity filter). One could note that, in contrast to AQP1, $c(z)$ is notably lower at the site of Tyr23 ($z \sim 2.5$ Å) in AQP0. The disruption of water chain caused by Tyr23 (Fig. 4d), which was determined in the earlier sections, could be responsible for the low water correlation at this region.

Bipolar water orientation, which is crucial for proton exclusion in AQPs [31], was also observed in our simulations of AQP1 and AQP0 (Fig. 4c), consistent with previous MD studies [10,12,20]. Although AQP1 and AQP0 present distinct dynamic behaviors, e.g., the water permeability and water distribution in the channel pore, in general, there seems little difference between AQP1 and AQP0 in the average water dipole orientation profiles, except a sharp valley in the profile of AQP0 around the region of Tyr23. The deep valley can be explained by the fact that water molecules form hydrogen bonds with the OH group of Tyr23 (see Fig. 4d), thus affecting the gesture of water. However, previous studies did not report a similar observation, probably due to the limited time scales (5 ns) of MD simulations [10,20].

In addition to the Tyr23 region that dominates the slow permeation of AQP0, another area that strongly affects the dynamic behaviors of water inside the AQP0 pore is the constriction region II which contains Tyr149 (see Fig. 2b). In this region, another significant interruption of water chain in AQP0 occurs, whereas the file is continuous in the corresponding region of AQP1 (Fig. 4a). Corresponding sharp changes in the water–water correlation (Fig. 4b) as well as in the water orientation (Fig. 4c) can also be observed in the profiles for AQP0 (compare to AQP1). Besides the narrow pore around this site limiting water transport, along the lines of a deduction provided in a recent study [18], it is the residue Tyr149 here that serves as a dynamic gate and interrupts the water chain inside the channel pore. The side chain of this residue exists in an alternative state at random between “up” and “down”, closing and opening the channel frequently during the simulation [18]. Hence, although Tyr149 is a less dominant determinant responsible for the slow permeation of AQP0 than Tyr23, it could also affect the water dynamics inside the AQP0 pore.

3.5. Interaction energies

The interactions of permeating water molecules with the environment play key roles in controlling the dynamic properties of water in AQPs [30,31,35]. As demonstrated in the previous sections, Tyr23 dominantly leads to the slow water permeation in AQP0, implying that the Tyr23 region in the AQP0 channel protein may generate a higher interaction energy barrier than other lumen-protruding residues such as Tyr149. To determine the interactions of water with the environment in more details, we studied the interaction energy between water passing through AQPs and its surroundings.

The coordinate data used to calculate interaction energies were collected every 20 ps over the last 60 ns simulation. One should note that a positive value of the interaction energy indicates a repulsive

interaction, whereas a negative one denotes an attractive interaction. In addition, the strength of the interaction is proportional to the absolute value of the interaction energy.

The interaction of a water molecule with the environment can be decomposed into the following contributions: from the channel protein, other water molecules within the channel pore, bulk water and the lipid bilayers. Since water inside the AQP pore is at long distances with bulk water and the lipids, it interacts weakly with them. Hence, for each position z we only investigated the water–protein interaction energy $\langle E_{W-P}(z)\rangle$ (also denoted as E_{W-P}), the water–water interaction energy $\langle E_{W-W}(z)\rangle$ (the permeating water molecule and other water molecules inside the channel pore; also denoted as E_{W-W}), and the total interaction energy, as $E_{W-Environment} = E_{W-P} + E_{W-W}$.

Fig. 5a shows a comparison of the total interaction energy $E_{W-Environment}$ of water inside AQP1 and AQP0. The interaction energy barrier in AQP0, which is defined as the difference between the

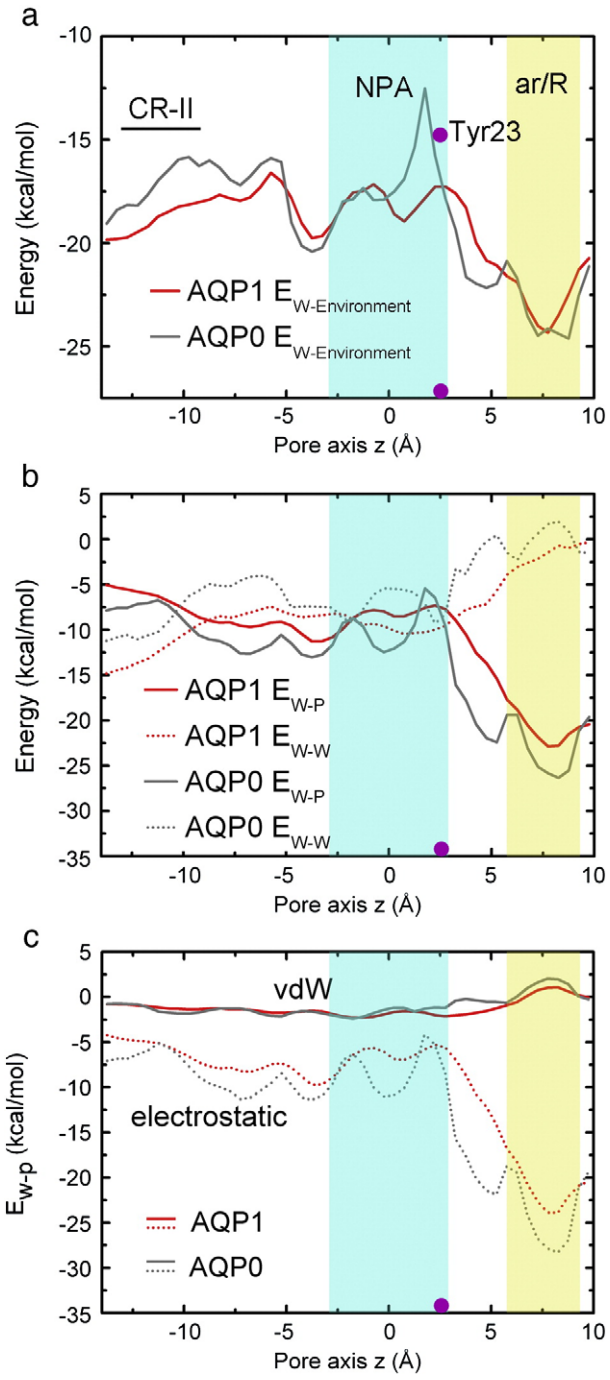

Fig. 5. Interaction energy of water inside the AQP channels with its surroundings. (a) Total interactions of water in the pores of AQP1 (red) and AQP0 (gray) with the environment. (b) Interactions of water with the channel protein (solid curve) and other water molecules within the channel pore (dotted curve). (c) Van der Waals (solid curve) and electrostatic (dotted curve) interaction between water and the channel protein.

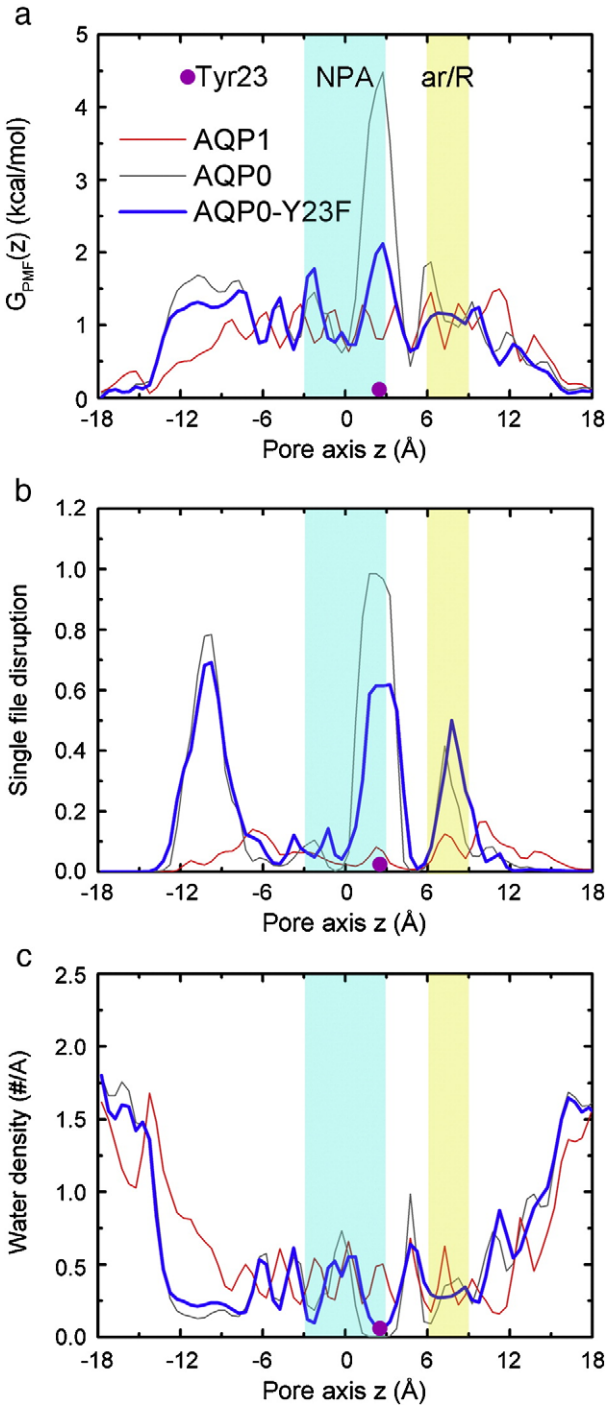

Fig. 6. Comparison of water dynamics inside the wild-type AQP0 and the Y23F mutant. (a) Free-energy profile. (b) Single file disruption. (c) Average water density. The profiles for AQP1 (thin red curve) and AQP0 (thin gray curve) in the three panels (a, b and c) correspond to the curves shown in Figs. 3d, 4a, and 3c, respectively, and the corresponding results for the AQP0-Y23F mutant are plotted in thick blue curves.

maximum and minimum of the energy profile, is 12.1 kcal/mol, which is 5.0 kcal/mol higher than that in AQP1. This difference suggests that more energy will be consumed for water transport in AQP0 than in AQP1, consistent with the fact that AQP0 is less permeable than AQP1. Moreover, two areas with remarkable peaks or valleys are noticed in the profiles. First, for both AQP1 and AQP0, the global minimum of the interaction energy appears at the conserved ar/R site. It suggests that water displays the strongest interaction with the environment at this position. The positively charged arginine at this site interacts with permeating water molecules strongly. Second, in the profile of AQP0, there is a sharp change around the position of Tyr23 (Fig. 5a), with a distinct peak (−12.5 kcal/mol) at its left side followed by a remarkably deep valley (−22.5 kcal/mol) at its right side, giving rise to a significant energy barrier (10.0 kcal/mol), while in the case of AQP1, no significant peak or valley around the NPA region can be observed. The high energy barrier around the Tyr23 site in AQP0 coincides exactly with the observed apparent disruption of water single file at this position (see Figs. 4a and d). Thus the remarkable energy barrier here should be attributed to the effect of Tyr23. Since the energy barrier here (10.0 kcal/mol) is comparable to the total barrier against water permeation (12.1 kcal/mol), the slow water permeation in AQP0 should be mainly caused by this residue. In contrast, around the residue Tyr149 of AQP0, which is part of the constriction region II, the AQP0 energy profile (Fig. 5a) is rather smooth. Hence, water can pass through the Tyr149 area more easily than the Tyr23 region, suggesting that Tyr149 is less important in limiting water transport than Tyr23.

The total interaction of water with the environment can be further decomposed into the water–protein and water–water interaction energies, as shown in Fig. 5b. For both AQP1 and AQP0, the water–protein interaction E_{W-P} (solid line) is negative, that is, the channel protein interacts attractively with water molecules within the pore interiors. In general, the water–protein interaction in AQP0 is stronger than that in AQP1 in most regions, which is owing to the narrower pore of AQP0. For AQP0, the water–protein interaction profile, similar to the total energy profile (Fig. 5a, gray line), has a significant peak and a deep valley around the Tyr23 region (Fig. 5b, solid gray line), mainly attributed to the electrostatic interaction (Fig. 5c), indicating that the water–protein interaction contributes dominantly to the huge energy barrier at this position. The trends of the E_{W-W} profiles for AQP1 and AQP0 (Fig. 5b, dotted lines) are nearly identical, however, the water–water interaction in AQP0 is much weaker than that in AQP1. Since water conduction in AQPs requires a collective translocation of the water single file, the weak interaction between adjacent waters in a water chain implies that AQP0 could exhibit a lower water permeability than AQP1.

3.6. Mutant MD simulation

Based on the above discussion, we have shown that a barrier dominantly caused by Tyr23 is responsible for the slow water conduction through AQP0. The role of Tyr23 in limiting water conduction can be further investigated by point mutation of this residue. We carried out an MD simulation of the AQP0-Y23F mutant by replacing the residue Tyr23 of AQP0 with phenylalanine, which differs from it only in the OH group of the side chain. Just as the wild-type, we also calculated the single channel water permeability P_f and made energy analyses for the mutant system. The calculated P_f value for the mutant is 1.9 ± 0.6 (also listed in Table 1). Compared to that of 0.5 ± 0.2 for the wild-type AQP0, the mutant transports water approximately three-fold faster. This can be explained from free-energy analyses. It is shown that the Y23F mutation significantly reduces the energy barrier at the mutation site (Fig. 6a) and reduces the local peak in the disruption of water file (Fig. 6b), although the overall water density is nearly identical to that in the wild-type AQP0 (Fig. 6c). This strongly demonstrates the fact again that Tyr23 is the primary residue responsible for the slow water permeation of AQP0.

4. Conclusions

In this study, the dynamics and energetics of water transport through AQP1, AQP0 and AQP0-Y23F mutant were investigated systematically based on MD simulations. It is shown that the residue Tyr23 dominantly leads to the notably lower water permeability of AQP0, compared to that of AQP1. This residue interrupts the single water file and forms a remarkably high barrier opposing water permeation through AQP0. A further mutation of Y23F in AQP0 can significantly reduce the energy barrier and lead to a 2- to 4-fold enhancement in water permeability, confirming the role of Tyr23 in lowering the water permeability of AQP0. Thus, we suggest a permeation experiment on the AQP0-Y23F mutant, and would expect a significant enhancement in water flow.

Acknowledgments

The work is supported by National and Jiangsu Province NSF (10732040, 10802037, 30970557, BK2008042) of China and the NUAA Funds (BCXJ08-02).

References

[1] P. Agre, Aquaporin water channels (Nobel Lecture), Angew. Chem. Int. Ed. 43 (2004) 4278–4290.
[2] P. Agre, The aquaporin water channels, Proc. Am. Thorac. Soc. 3 (2006) 5–13.
[3] M. Borgnia, S. Nielsen, A. Engel, P. Agre, Cellular and molecular biology of the aquaporin water channels, Annu. Rev. Biochem. 68 (1999) 425–458.
[4] K. Murata, K. Mitsuoka, T. Hirai, T. Walz, P. Agre, J.B. Heymann, A. Engel, Y. Fujiyoshi, Structural determinants of water permeation through aquaporin-1, Nature 407 (2000) 599–605.
[5] H. Sui, B.G. Han, J.K. Lee, P. Walian, B.K. Jap, Structural basis of water-specific transport through the AQP1 water channel, Nature 414 (2001) 872–878.
[6] W.E. Harries, D. Akhavan, L.J.W. Miercke, S. Khademi, R.M. Stroud, The channel architecture of aquaporin 0 at a 2.2-Å resolution, Proc. Natl. Acad. Sci. U. S. A. 101 (2004) 14045–14050.
[7] T. Gonen, P. Sliz, J. Kistler, Y. Cheng, T. Walz, Aquaporin-0 membrane junctions reveal the structure of a closed water pore, Nature 429 (2004) 193–197.
[8] T. Gonen, Y. Cheng, P. Sliz, Y. Hiroaki, Y. Fujiyoshi, S.C. Harrison, T. Walz, Lipid–Protein interactions in double-layered two-dimensional AQP0 crystals, Nature 438 (2005) 633–638.
[9] D. Fu, A. Libson, L.J. Miercke, C. Weitzman, P. Nollert, J. Krucinski, R.M. Stroud, Structure of a glycerol-conducting channel and the basis for its selectivity, Science 290 (2000) 481–486.
[10] M. Hashido, M. Ikeguchi, A. Kidera, Comparative simulations of aquaporin family: AQP1, AQPZ, AQP0 and GlpF, FEBS Lett. 579 (2005) 5549–5552.
[11] B.G. Han, A.B. Guliaev, P.J. Walian, B.K. Jap, Water transport in AQP0 aquaporin: molecular dynamics studies, J. Mol. Biol. 360 (2006) 285–296.
[12] B.L. de Groot, H. Grubmüller, Water permeation across biological membranes: mechanism and dynamics of aquaporin-1 and GlpF, Science 294 (2001) 2353–2357.
[13] B.L. de Groot, H. Grubmüller, The dynamics and energetics of water permeation and proton exclusion in aquaporins, Curr. Opin. Struct. Biol. 15 (2005) 176–183.
[14] M.Ø. Jensen, E. Tajkhorshid, K. Schulten, Electrostatic tuning of permeation and selectivity in aquaporin water channels, Biophys. J. 85 (2003) 2884–2899.
[15] B.L. de Groot, T. Frigato, V. Helms, H. Grubmüller, The mechanism of proton exclusion in the aquaporin-1 water channel, J. Mol. Biol. 333 (2003) 279–293.
[16] G. Chandy, G.A. Zampighi, M. Kreman, J.E. Hall, Comparison of the water transporting properties of MIP and AQP1, J. Membr. Biol. 159 (1997) 29–39.
[17] G.M. Preston, T.P. Carroll, W.B. Guggino, P. Agre, Appearance of water channels in *Xenopus* oocytes expressing red cell CHIP28 protein, Science 256 (1992) 385–387.
[18] M.Ø. Jensen, R.O. Dror, H. Xu, D.W. Borhani, I.T. Arkin, M.P. Eastwood, D.E. Shaw, Dynamic control of slow water transport by aquaporin 0: implications for hydration and junction stability in the eye lens, Proc. Natl. Acad. Sci. U. S. A. 105 (2008) 14430–14435.
[19] P. Francis, V. Berry, S. Bhattacharya, A. Moore, Congenital progressive polymorphic cataract caused by a mutation in the major intrinsic protein of the lens, MIP (AQP0), Br. J. Ophthalmol. 84 (2000) 1376–1379.
[20] M. Hashido, A. Kidera, M. Ikeguchi, Water transport in aquaporins: osmotic permeability matrix analysis of molecular dynamics simulations, Biophys. J. 93 (2007) 373–385.
[21] W. Humphrey, A. Dalke, K. Schulten, VMD: visual molecular dynamics, J. Mol. Graph. 14 (1996) 33–38.

[22] L. Kalé, R. Skeel, M. Bhandarkar, R. Brunner, A. Gursoy, N. Krawetz, J. Phillips, A. Shinozaki, K. Varadarajan, K. Schulten, NAMD2: greater scalability for parallel molecular dynamics, J. Comp. Phys. 151 (1999) 283–312.
[23] A.D. MacKerell Jr., D. Bashford, M. Bellott, R.L. Dunbrack Jr., J.D. Evanseck, M.J. Field, S. Fischer, J. Gao, H. Guo, S. Ha, D. Joseph-McCarthy, L. Kuchnir, K. Kuczera, F.T.K. Lau, C. Mattos, S. Michnick, T. Ngo, D.T. Nguyen, B. Prodhom, W.E. Reiher, B. Roux III, M. Schlenkrich, J.C. Smith, R. Stote, J. Straub, M. Watanabe, J. Wiorkiewicz-Kuczera, D. Yin, M. Karplus, All-atom empirical potential for molecular modeling and dynamics studies of proteins, J. Phys. Chem. B 102 (1998) 3586–3616.
[24] W.L. Jorgensen, J. Chandrasekhar, J.D. Madura, R.W. Impey, M.L. Klein, Comparison of simple potential functions for simulating liquid water, J. Chem. Phys. 79 (1983) 926–935.
[25] U. Essmann, L. Perera, M.L. Berkowitz, T. Darden, H. Lee, L.G. Pedersen, A smooth particle mesh Ewald method, J. Chem. Phys. 103 (1995) 8577–8593.
[26] S.E. Feller, Y. Zhang, R.W. Pastor, B.R. Brooks, Constant pressure molecular dynamics simulation: the Langevin piston method, J. Chem. Phys. 103 (1995) 4613–4621.
[27] F. Zhu, E. Tajkhorshid, K. Schulten, Collective diffusion model for water permeation through microscopic channels, Phys. Rev. Lett. 93 (2004) 224501.
[28] M.Ø. Jensen, O.G. Mouritsen, Single-channel water permeabilities of *Escherichia coli* aquaporins AqpZ and GlpF, Biophys. J. 90 (2006) 2270–2284.
[29] D.F. Savage, P.F. Egea, Y. Robles-Colmenares, J.D. O'Connell, R.M. Stroud, Architecture and selectivity in aquaporins: 2.5 Å x-ray structure of aquaporin Z, PLOS Biol. 1 (2003) 334–340.
[30] J.S. Hub, B.L. de Groot, Mechanism of selectivity in aquaporins and aquaglyceroporins, Proc. Natl. Acad. Sci. U. S. A. 105 (2008) 1198–1203.
[31] E. Tajkhorshid, P. Nollert, M.Ø. Jensen, L.J. Miercke, J. O'Connell, R.M. Stroud, K. Schulten, Control of the selectivity of the aquaporin water channel family by global orientational tuning, Science 296 (2002) 525–530.
[32] G. Hummer, J.C. Rasaiah, J.P. Noworyta, Water conduction through the hydrophobic channel of a carbon nanotube, Nature 414 (2001) 188–190.
[33] F. Zhu, E. Tajkhorshid, K. Schulten, Theory and simulation of water permeation in aquaporin-1, Biophys. J. 86 (2004) 50–57.
[34] J.B. Heymann, A. Engel, Aquaporins: phylogeny, structure, and physiology of water channels, News Physiol. Sci. 14 (1999) 187–193.
[35] M.Ø. Jensen, S. Park, E. Tajkhorshid, K. Schulten, Energetics of glycerol conduction through aquaglyceroporin GlpF, Proc. Natl. Acad. Sci. U. S. A. 99 (2002) 6731–6736.
[36] M.L. Zeidel, S.V. Ambudkar, B.L. Smith, P. Agre, Reconstitution of functional water channels in liposomes containing purified red cell CHIP28 protein, Biochemistry 31 (1992) 7436–7440.
[37] T. Walz, B.L. Smith, M.L. Zeidel, A. Engel, P. Agre, Biologically active two-dimensional crystals of aquaporin CHIP, J. Biol Chem. 269 (1994) 1583–1586.
[38] M.L. Zeidel, S. Nielsen, B.L. Smith, S.V. Ambudkar, A.B. Maunsbach, P. Agre, Ultrastructure, pharmacologic inhibition, and transport selectivity of aquaporin channel-forming integral protein in proteoliposomes, Biochemistry 33 (1994) 1606–1615.
[39] B. Yang, A.S. Verkman, Water and glycerol permeabilities of aquaporins 1-5 and MIP determined quantitatively by expression of epitope-tagged constructs in *Xenopus oocytes*, J. Biol. Chem. 272 (1997) 16140–16146.
[40] A.B. Mamonov, R.D. Coalson, M.L. Zeidel, J.C. Mathai, Water and deuterium oxide permeability through aquaporin 1: MD predictions and experimental verification, J. Gen. Physiol. 130 (2007) 111–116.
[41] O.S. Smart, J.G. Neduvelil, X. Wang, B.A. Wallace, M.S.P. Sansom, HOLE: a program for the analysis of the pore dimensions of ion channel structural models, J. Mol. Graph. 14 (1996) 354–360.